Title

Subtitle

by

Mikkel Metzsch Jensen

THESIS

for the degree of

MASTER OF SCIENCE

Faculty of Mathematics and Natural Sciences
University of Oslo

Spring 2023

Title

Subtitle

Mikkel Metzsch Jensen

© 2023 Mikkel Metzsch Jensen

Title

http://www.duo.uio.no/

Printed: Reprosentralen, University of Oslo

Abstract

Abstract.

Acknowledgments

Acknowledgments.

Contents

List of symbols?

Maybe add list of symbols and where they are used like Trømborg.

Introduction

0.1 Motivation

0.1.1 Friction

Friction is a fundamental force that takes part in almost all interactions with physical matter. Even though the everyday person might not be familiar with the term "friction" we would undoubtedly notice its disappearing. Without friction, it would not be possible to walk across a flat surface, lean against the wall or secure an object by the use of nails or screws (Static friction allows us to join objects together using screws [1][p. 5]). Similarly, we expect a moving object to eventually come to a stop if not supplied with new energy, and we know intuitively that sliding down a snow covered hill is much more exciting than its grassy counterpart. It is probably safe to say that the concept of friction is well integrated in our everyday life to such an extent that most people take it for granted. However, the efforts to control friction dates back to the early civilization (3500 B.C.) with the use of the wheel and lubricants to reduce friction in translational motion [2]. Friction is a part of the wider field tribology derived from the Greek word *Tribos* meaning rubbing and includes the science of friction, wear and lubrication [2].

The most important motivation to study tribology is ultimately to gain full control of frictional and wear for vairous technical applications. Especially, reducing friction is of great interest as this has tremendous advantages regarding energy effeciency. It has been reported that that monetary value of tribological problems has significant potential for economic and environmental improvements [3]:

> "On global scale, these savings would amount to 1.4% of the GDP annually and 8.7% of the total energy consumption in the long term." [4].

The reduction of friction is not the only sensible application as a controlled increase in friction might be of interest in the development of grasping robots or perhaps breaking system (get some sourced examples maybe...).

To the best of my knowdelegde kirigami has not yet been implemented to alter the friction properties in a similar manner as done in this thesis.

0.1.2 Thesis

In this thesis we investigate the possibility to control the frictional properties of a graphene sheet by applying strategically positioned cuts to the sheet inspired by kirigami. Kirigami is a variation of origami where the paper is cut additionally to being folded. Hanakata et al. [5] has shown that kirigami inspired cuts on a graphene sheet can be used to alter the yield strain and yield stress of the sheet. They observed that the stretching of the cutted sheet induced a out-of-plane buckling which serves as a key observation for the motivation of this thesis. It is currently well established/believed that the friction between two surfaces is proportional to the real microscopic contact area (source here?). Hence, one can hypothesize that the buckling of the sheet will affect the contact area and consequently the frictional properties.

0.2 Approach

In the study by Hanakata et al. [5] they used a machine learning (ML) approach to overcome the complexity of the nonlinear effects arrising from the out-of-plane buckling which made them succesfully map the cutting patterns to the mechanical properties of yield and stress. The dataset used for the ML training was generated by molecular dynamics (MD) simulations for a limited set of cut configuration. By training the network the

MD simiulaitons could effectively be skipped all together making for an accelerated search through new cut configurations for certain mechanical properties. By setting up a MD simulation that qunatifies the frictional properties of the graphene sheet we aim to make an analog study regarding the search for certain frictional properties.

We will take this on step further by creating a GAN network that utilises the latter network for creating an inverse design framework. That is, a network that takes frictional properties as input and return the corresponding cut configuration. By having such a tool we can execute a targeted search for exotic frictional properties. Particularly, we are interested in nonlinear and possibly even negative friction coefficients. Friction is essentially observed to increase with increasing load on the frictional surface, and we often describe this as having a positive friction coefficient. However, if we are able to couple the stretching of the sheet with friction we might be able to break this barrier for the coefficient. By imagining some nanomachine which translates downward pressure into either compression of expansion of the altered graphene, we could have a coupling between downward pressure and stretch of the sheet. In that case, a friction force depending on stretch could effectively be made to decrease with increasing load which would correspond to a negative friciton coeffcient following this definition (formulate such that we do not imply free acceleration from nothing).

One of the features from inverse design, seperating it from the general class of ML approaches, is that we do not depend on trusting the ML predictions. While a standard neural network might be extremely efficient on a certain prediciton task we have usually no information on how these predictions are based. We say that the internal workings of the network is a black box beyond our capacaity of interpretation. However, for the inverse design problem we are prompted with a few promising design propsals which can immediately be tested in the MD simulations which we will regard as the most reliable predictor in this setting. Hence, if arriving at a successful design in alignment our search prompt, we can disregard any uncertainty in the network. In that case the remaining gap to bridge is that of the MD simulation and real life implementations.

0.3 Objective of the study

1. Design a MD simulation to evaluate the frictional properties of the grpahene sheet under different variations of cut patterns, stretching and loading, among other physical variables.
2. Train a network to replace the MD simulation completely.
3. (Variation 1) Do an accelerated search using the ML network for exotic frictional properties such as low and friction coeffcients and a strong coupling between stretch and friction.
4. (Variation 2) Make a GAN network using the first network and predict cut configurations for some of the above mentiond frictional properties.
5. (If I have time) Make a nanomachine that couples load and stretch (perhaps just artificially without any molecular mechanism) to test the hypothesize of a negativ friction coefficient.

0.4 Contributions

What did I actually achieve

0.5 Thesis structure

How is the thesis structured.

Simulations

0.6 Baseline study (find better name)

Consider relabeling drag length to sliding distance instead.

0.6.1 Friction simulation parameters

The friction simulation is governed by a set of parameters where some is kept constant while other is varied to gain insight in the frictional properties. These parameters can be categorised into three main categories of different purpose as described in table 1.

Table 1: Parameters of the numerical procedure for measuring friction.

Category	Parameter name: description	Category purpose
Physical	- T: Temperature for the Langevin thermostat. - v_{slide} : Sliding speed for the sheet translation. - K: Spring constant for the spring force between the virtual atom and the pull blocks responsible for translating the sheet along the substarte. An infinte spring constant is achieved by moving the pull blocks as a rigid body (Lammps: fix move). - Scan angle: The direction for which we translate the sheet.	Parameters expected to have a physical effect on the friction properties, which is kept fixed and thus not included in the machine learning input set.
Measurement	- dt: Integration timestep. - t_R: Relaxtion time before strething. - Pauses between stretch and adding normal force and between dragging the sheet. - Stretch Speed: How fast to stretch the sheet. - Slide distance: How far to translate the sheet. - Sheet size: Spatial size of the 2D sheet. - Pull block size.	Paramters influecing the simulation dynamics and being representative of the experimental procedure that we are mimicking. These parameters is chosen with the aim of getting stable parameters under small perturbations of the given parameter.
ML input	- Sheet configuration: A binary matrix containing information of which atoms are removed (0) and which is still present (1) in the graphene sheet. - Stretch amount: The relative sheet stretch in percentage. - F_N: Applied normal force to the pull blocks.	The remaining paramters serves as input variables for optimization process and is thus given as input variables for the machine learning (ML).

Due to the great number of parameters, and corresponding range of reasonable numerical values they can take, it is ... to parameter search including all of these. Thus, we will to a great extent rely on a reverse engineering in order to establish a set of parameters for the *physical* and *measurement* categories along with numerical ranges for the *ML input* category which gives stable and promising results. By doing so we effectively narrow down the parameter regime for which the investigated frictional properties belong. We aim to chose the parameters in order to accomodate a balance between generlizable and stable result which is simmutaneously a suting candidate as a proof of concept for the control of friction properties using kirigami inspired cuts.

In the following we present the results of the friction simulations in parallel to the procedure of investigating the choice of different parameters.

In the following subsections (X to Y) we are going to present the friction simulation results in parallel to the presentation of the reasoning behind the parameter choices. For this we will refer to the default parameter choice showcased in table 2 which is representative of the final parameter choices.

Table 2: Final parameters for the friction simmulations Probably not the neatest way format for this...

Physical	Measurements	ML input
$T = 300\,\mathrm{K}$ $v_{\text{slide}} = 20\,\mathrm{m/s}$ $K = \inf$ (LAMMPS: *fix move*) Scan angle : $(x, y) = (0, 1)$	$dt = 1\,\mathrm{fs}$ $t_R = 15\,\mathrm{ps}$ Pauses $= 5\,\mathrm{ps}$ Stretch speed $= 0.01\,\mathrm{ps}^{-1}$ Slide distance $= 400\,\text{Å}$ Sheet size $= 130.029 \times 163.219\,\text{Å}$ Pull block size $= 2 \times 130.029 \times 15.183\,\text{Å}$	Sheet configuration = Contiguous Stretch amount = Below rupture $F_N = [0.1, 10]$ nN

Say someting about how these parameters is chosen. Reference to articles for which these was mirrored from.

0.6.1.1 Pressure reference for normal load domain

Find place to put this.

In order to relate the magntidue of the normal force in our friciton measurement we will use the pressure as a reference. We will use the pressure underneath a stiletto shoe as a worst case for human pressure execuation underneath the shoes. From (source 1) it is reported that the diameter of a stiletto heeled shoe can be less than 1 cm. Hence a 80 kg man[1] standing on one stiletto heel (with all the weight on the heel) will result in a pressure

$$P = \frac{F}{A} = \frac{mg}{r^2\pi} = \frac{80\,\mathrm{kg} \cdot 9.8\,\frac{\mathrm{m}}{\mathrm{s}^2}}{(\frac{1 \times 10^{-2}\,\mathrm{m}}{2})^2\pi} = 9.98\,\mathrm{MPa}$$

While this is in itself a spectacular realization that is often used in introductory physics courses (source 2) to demonstrate the rather extreme pressure under a stiletto heel (greater than the foot of an elephant) (how many Atmos?) this serves as a reasonible upperbound for human executed pressure. With a full sheet area of $\sim 21 \times 10^3\,\text{Å}^2$ we can achieve a similar pressure of $\sim 10\,\mathrm{MPA}$ with a normal force of

$$F_N = 10\,\mathrm{MPa} \cdot 21 \times 10^{-17}\,\mathrm{m}^2 = 2.10\,\mathrm{nN}$$

Of course this pressure might be insufficient for various industrial purposes, but with no specific procedure in mind this serves as a decent reference point. Notice that if we consider a human foot with ares $113\,\mathrm{cm}^2$ the pressure drops to a mere $70\,\mathrm{kPa}$ corresponding to $\sim 0.01\,\mathrm{nN}$.

[1] Yes, a man can certainly wear stilleto heels.

0.6.2 Single friction simulation analysis

We begin by assessing the raw data for a single friction simulation run with the default parameters shown in table 2 for a non-cut sheet, no stretch and an applied normal force of 1 nN.

0.6.2.1 Force oscillations

We first assess the raw data for the friction force $F_\parallel$ parallel to the drag direction as seen in figure 1. The sample rate is 10 ps^{-1} = 100 timesteps^{-1} for which each sample is the mean value of the 100 timesteps preceding the given sample interval. We observe immediately that the data carriers oscillations on different time scales. By applying a savgol filter to the data with a polyorder of 5 and window length of 150 timesteps, corresponding to a sliding distance of 3 Å or a time window of 15 ps, we can qualitatively point out at least two different frequencies of osccilation. On figure 1a we see roughly three waves on the savgol filter corresponding to a relative high frequency, while on 1b the same savgol filter reveals a lower frequency on top of the first, creating the visual pattern of a wavepacket.

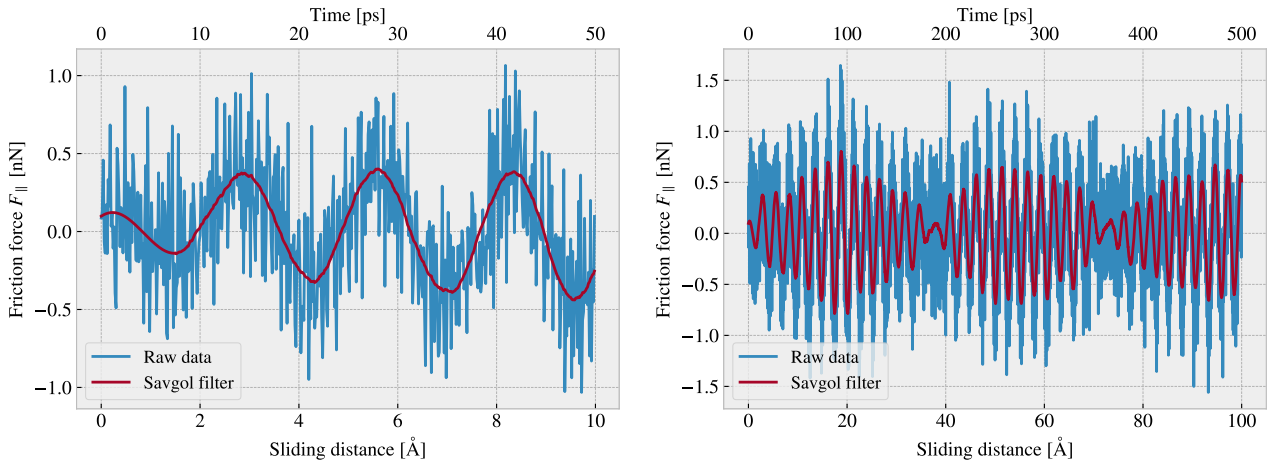

(a) Drag length of 10 Å.

(b) Drag length of 100 Å.

Figure 1: Friction force $F_\parallel$ with respect to the drag direction between (full) sheet and substrate versus sliding distance. The sliding distance is measured by the constant movement of the virtual atom and not the COM of the sheet. However, we expect these measures to be fairly identical due the fact that the pull blocks is rigidly coupled to the virtual atom. The red line represents a savgol filter with window polyorder 5 and window length of 150 timesteps (corresponding to a sliding distance of 3 Å or a time window of 15 ps).

By performing a Fourier Transform (FT) on the data we can quantify the leading frequencies as seen in figure 2a. By plotting the two most dominant frequencies $f_1 = 0.0074$ ps^{-1} and $f_2 = 0.0079$ ps^{-1} as $\sin(2\pi f_1) + \sin(2\pi f_2)$ we find a qualitatively convincing fit to the observed wavepacket shape as seen in figure 2b. By using the trigonometric identity

$$\sin(\alpha+\beta) = \sin(\alpha)\cos(\beta) + \cos(\alpha)\sin(\beta),$$
$$\sin(\alpha-\beta) = \sin(\alpha)\cos(\beta) - \cos(\alpha)\sin(\beta),$$

and decomposing $f_1 = a - b$, $f_2 = a + b$ we can rewrite the sine sum as the sinusoidal product

$$\begin{aligned}\sin(2\pi f_1)\sin(2\pi f_2) &= \sin\big(2\pi(a-b)\big)\sin\big(2\pi(a+b)\big)\\ &= \sin(a)\cos(b) + \cancel{\cos(2\pi a)\sin(2\pi b)} + \sin(2\pi a)\cos(2\pi b) - \cancel{\cos(2\pi a)\sin(2\pi b)}\\ &= 2\sin(2\pi a)\cos(2\pi b),\end{aligned}$$

with

$$a = \frac{f_1+f_2}{2} = 0.0763 \pm 0.0005\,\text{ps}^{-1}, \qquad b = \frac{f_2-f_1}{2} = 0.0028 \pm 0.0005\,\text{ps}^{-1},$$
$$= 0.381 \pm 0.003\,\text{Å}^{-1}, \qquad = 0.014 \pm 0.003\,\text{Å}^{-1},$$

where the latter frequency is denoted with respect to the sliding distance. This makes us recognize the high osccilation frequency as a and the low frequency as b. The faster one has a period of $T_a = 2.62 \pm 0.02$ Å[2]. This corresponds well with the magnitude of the lattice spacing and especialy that of graphene at 2.46 Å as expected theoretically (make reference to theory section?). We also take note of the longest period $T_b = 71 \pm 15$ Å^{-1} which will be relevant for the evaluation of measurement uncertainty in section 0.6.3.

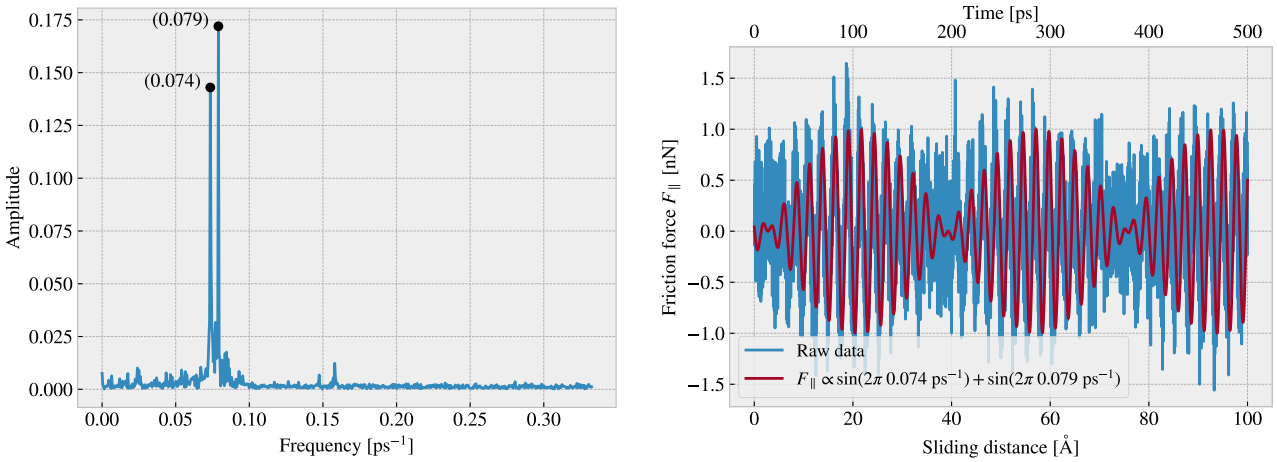

(a) FT result shown for a reduced frequency range.

(b) Two most dominant frequencies applied to the data from figure 1b

Figure 2: Fourier transform (FT) analysis of the full friction force data (all 400 Å sliding distance) shown in figure 1. (a) shows the two most dominant frequency peaks. Note that no significant peaks was found in a higher frequency than included here. (b) shows a comparison between the raw data and the wavefunction corresponding to the two peaks in figure (a).

0.6.2.2 Decompositions

In the previous analysis we have looked only at the friction force for the full sheet, including the pull blocks which is locked off during sliding, and with respect to the drag direction. This represents our choice measurement which we will adress in the following.

Due to the fact that we are only applying cuts to the inner sheet (excluding the pull blocks), it might seem more natural to only consider the friction on that part. If the desired frictional properties can be achieved by altering the inner sheet one can argue that any opposing effects from the pull blocks can be mitigated by scaling the relative size between the inner sheet and the pull blocks. However, when looking at the time series of the friction force decomposed with respect to the inner sheet and pull block region (see figure 3a), we observe the friction force arrising from those parts are seemingly antisymmetric. That is, the distribution of the fricitonal pull from the substrate on the sheet is oscillating between the inner sheet and the pull block. Keeping in mind that normal force is only applied to the pull blocks we might take this as an integrated feature of the system which does not nessecary dissapear when changing the spatial ratio between inner sheet and pull block. Any interesting friciton properties might depend on this internal distribution of forces. Hence, we hedge our bets and use the full sheet friction force as a hollistic approach to this measurement problem.

Similar we might question the decision of only considering the frictional force projected onto the sliding direction as we are neglecting the "side shift" induced during the slide phase. In figure 3b we see the decomposition into force components parallel $F_\parallel$ and perpendicular $F_\perp$ to the slide direction respectively. We see that the most dominant trends is projected into the parallel component. If we want to include the perpendicular component as well we would have to evaluate the friction as the length of the force vector for which we would lose the sign of the force direction. Hence, we would only get a positive contributin which would not be able to capture the change between resisting and assisting the sliding during stick-slip motion. One option to accommodate this is by using the vector length but keeping the sign from the projection parallel to the sliding direction. However, we

[2]The uncertainty Δy is calculated as $\Delta y = \left|\frac{\partial y}{\partial x}\Delta x\right|$ for uncertainty Δx and $y(x)$

omit such compromises as this might make analysis interpration more difficult, and we use only the parallel component going forward.

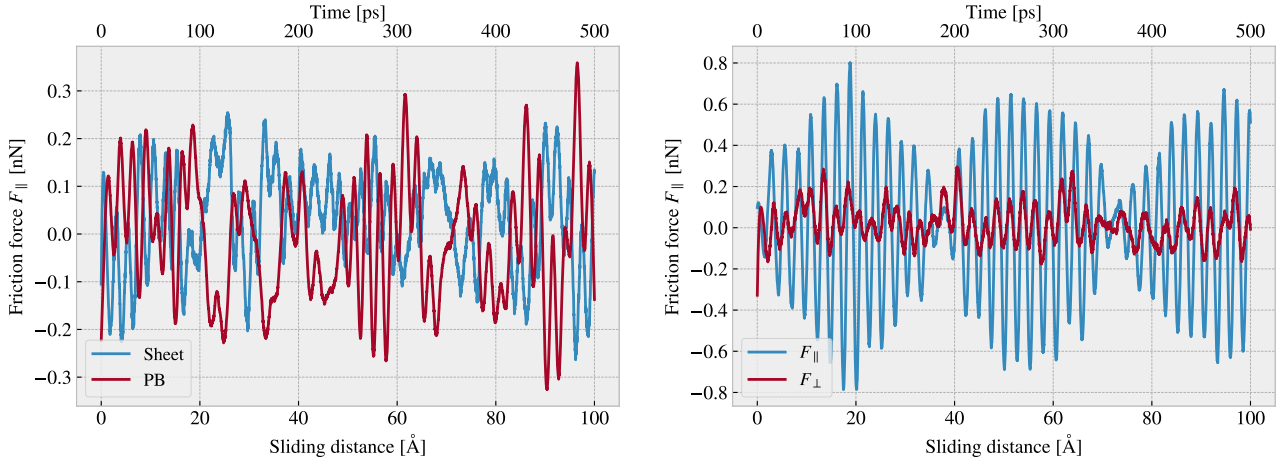

(a) Decomposition into group inner sheet (sheet) and pull blocks (PB).

(b) Decomposition into parallel ($F_\parallel$) and perpendicular ($F_\perp$) to drag sliding direction.

Figure 3: Friction force decomposition on the data shown in figure 1 with applied savgol filters similar to that of figure 1b with window polyorder 5 and window length of 150 timesteps (corresponding to a sliding distance of 3 Å or a time window of 15 ps).

0.6.2.3 Center of mass path

From the previous observations of the friction force time series we see evidence of a stick-slip behvaiour. Specially, we see in figure 3b that this might be the case both parallel and perpendicular to the sliding direction. By looking at the x, y-position for the sheet center of mass (COM) we observe the stick-slip motion manifested as a variation in COM speed combinned with a side to side motion as shown in figure 4*a*. In an attempt to increase the magnitude of the slips we evaluate a similar simulation with spring contant $K = 30\,\mathrm{N/m}$ (see figure 4b) in contrast to that of an infinte spring constant. While the maximum slip speed stays within a similar order of magnitude the slip length in the sliding direction is increased along with the side to side motion. Note that the axis scale is different between figure 4a and 4a. However, in both cases we observe that the side to side motion is associated with a low speed, meaning that is more reminiscent of a "slow" creep alignment with the substrate than a slip.

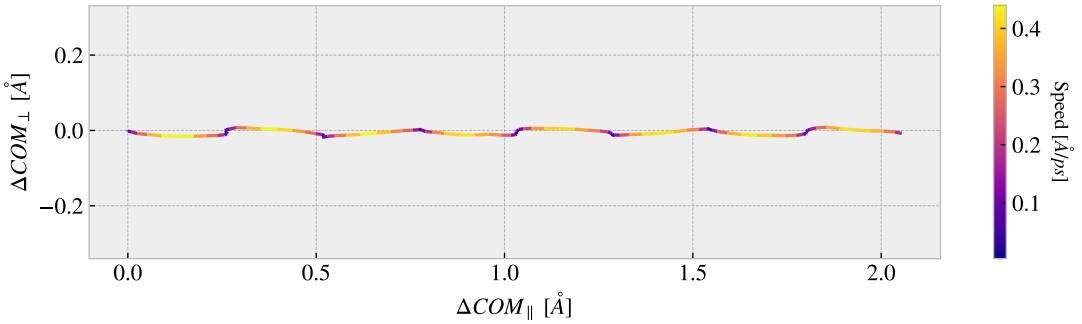

(a) $K = \inf$ (Fix move)

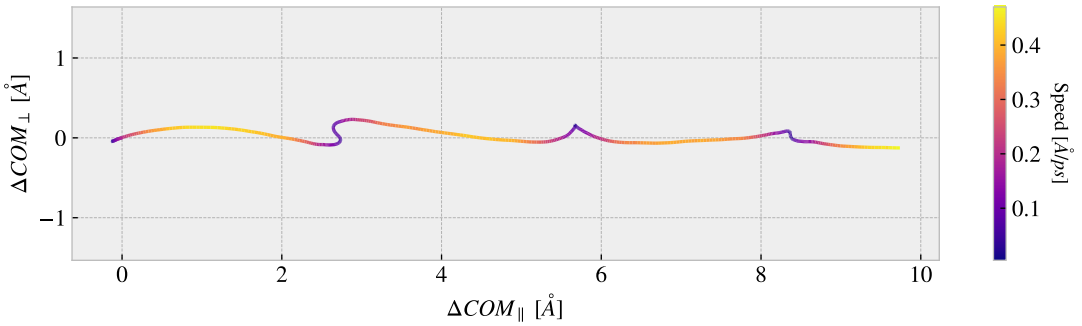

(b) 30 N/m

Figure 4: Center of mass posotion relative to the start of the sliding phase in terms of the direction parallel to the sliding direction $\Delta COM_\parallel$ and the axis perpendicular to the sliding direction $\Delta COM_\perp$. The colorbar denotes the absolute speed of the COM.

0.6.3 Defining metrics for dynamic and static friction

In order to evaluate the frictional properties of the sheet we reduce the comprehensive friction force time series adressed in section 0.6.2 into single metrics describing the dynamic and static friciton. The natural choice is to use the mean and max values of the time series.

0.6.3.1 Dynamic friction

For the dynamic friction measurement we take the mean value of the latter half of the dataset to ensure that we are sample from a stable system. For a full sliding simulation of 400 Å we thus base our mean value on the latter 200 Å of sliding. In figure 5a we have shown the friction force of the first 10 Å of sliding together with a running mean with window length of 5 Å corresponding to 50% the data length. This is merely done to illustrate the samplig procedure and by only using a 10 Å sliding distance the final mean estimate (indicated with a dot) takes a negative value due to the specific cut-off of the few oscialltion captured here. Nonetheless, one approach to quanity the uncertainy of the final mean estimate is to consider the variation of the running mean preceeding the final mean value. The more the running mean fluctuates the more uncertainty associated with the final estimate. However, only the running mean "close" to the ending should be considered, since the first part will rely on data from the beginning of the simulation. From the Fourier analyse in section 0.6.2.1 we found the longest significant oscillation period to be ~ 71 Å^{-1} corresponding to $\sim 35\%$ of the running mean window consisting of 200 Å of slifing when including all the data. Hence, we use the standard deviation of the final 35% of the running mean to approximate the uncertainty of the final mean value, and we estimate the relative error by dividing the standard deviation by the final mean value. In figure 5b we showcase a running standard deviation of a window length 35% the running mean window in figure 5a for the illustrative case of a total 10 Å slide. The final uncertainty value is marked by a dot, and we see as expected that we get a high relative error of $\sim 257\%$ which corresponds well with the short sampling period and the mean value taking an unphysical negative value.

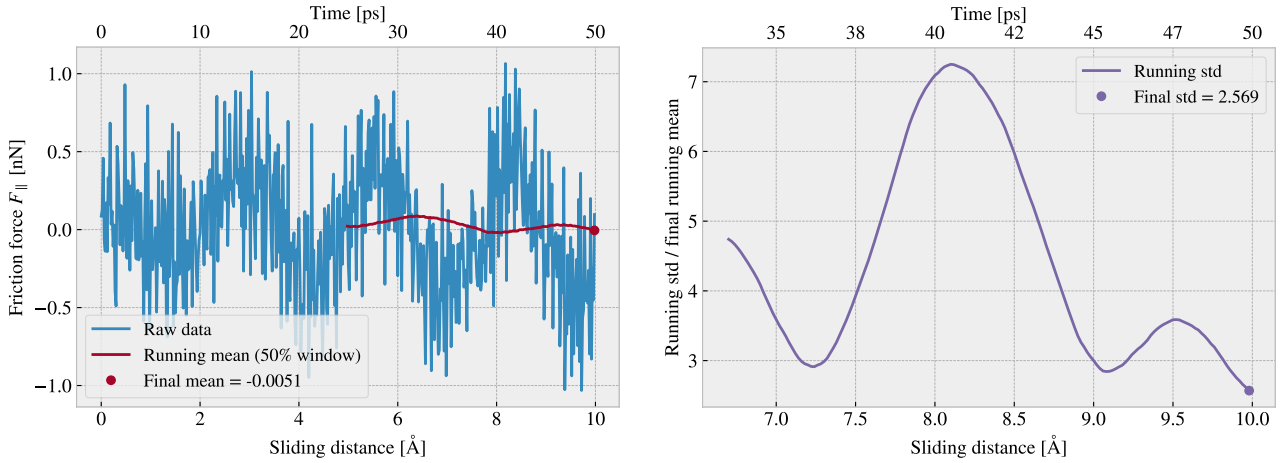

(a) Running mean with window length 5 Å (50% the data length).

(b) Running std with window length 1.75 Å (35% the mean window length.)

Figure 5: Running mean and running standard deviation (std) on the friction force data from a 10 Å of sliding simulation. The running mean window is 50% the data length while the running std window is 35% the running mean window length.

When including the full dataset of 400 Å of sliding, such that std window actually matches with the longest period of oscillations expected from the data, we get a final relative error of $\sim 12\%$ as shown in fig 6. This is arguable just at the limit for an acceptable error, but as we shall see later (Make a reference to fig or sec) this high relative error is mainly connected to the cases of low friction. When changing the simulation parameters, such that the mean friction evaluates to considerable higher values, the relative error drops to the order (put in numbers). One interpration of this finding is simply that the oscialltiosn in the running mean is somewhat independent of the magnitude of the friction. In that case, the relative error will spike for the low friction cases.

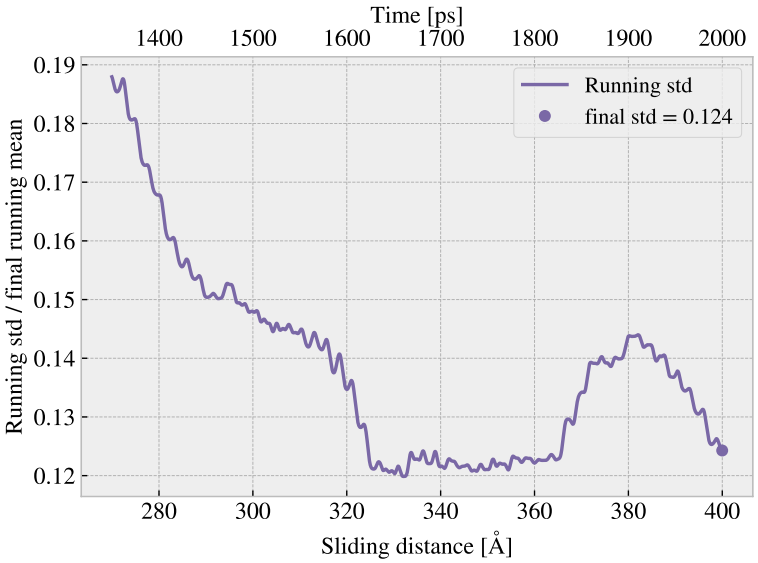

Figure 6: Running standard deviation (std) for a full 400 Å sliding simulation. The running std window is 70 Å (35% the running mean window of 50% the data length).

0.6.3.2 Static friction

The max value is the most obvious choice for adressing the static friction, even though that the definition of the static friction is a bit vague. When considering the friction force time series in figure 1 we observe that the

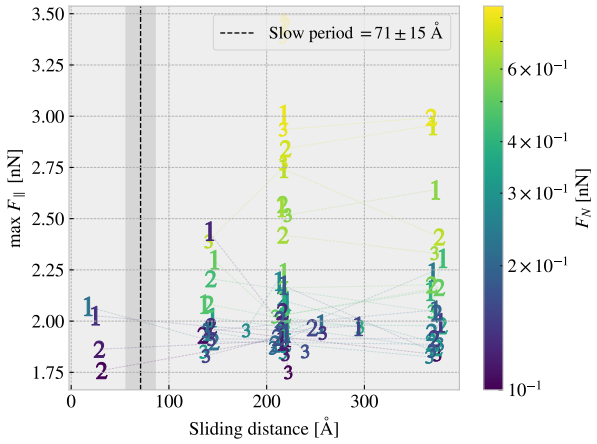

Figure 7: Distribution of top three max friction force peaks for 30 uniformly sampled normal forces $F_N \in [0.1, 10]$ nN. The dotted line and the grey area marks the slowest significant oscialltion period found in the data and thus marking a dividing line for whether a peak falls within the "beginning" of the sliding simulation.

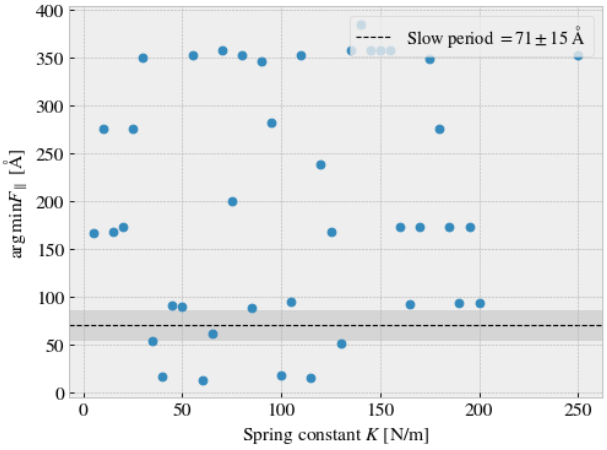

Figure 8: Sliding displacement for the max friction peak to appear as a function of spring constant. Fix-move is tmp mapped to K = 200 here without any discontinuous lines.

stick-slip oscillations increase in magnitude toward a global peak at ~ 20 Å. Thus, we could identify this peak as the static friction force, but the global max does in fact rarely fall within the first part of the sliding. In figure 7 we investigate the top three max value, at which sliding distance they accour and at what magnitude, for 30 uniformly sampled normal forces in the interval $[0.1, 10]$ nN. It is immediately clear that only few of the peaks falls within the "beginning" of the simulation defined by the slowest significant oscialltion period of 71 ± 15 Å. In fact only 2/30 global values and 4/90 top three values can be associated to the start of the sliding by this definition. Thus, this result suggest that the max value cannot be used as a reliable measure for the static friction either due to its lack of presence or due to the simulation setup procedure. For a more typycal evaluation of the static friction force one would increase force slowly until the first slip significant slip is recorded (a series of precursors is expected to precede this). In our simulations we drag the sheet relatively fast in a rigid matnner which made ..remove... the statuic friction phenonema. Find reference stating that static friction might dissapear when increasing the spring constant of the probe to stiff. By changing the spring constant we investigate possibility to observe a static friction response within the framework of our simulation procedure as shown in figure 8. However, the results do not indicate any implications that a recognizable domain exist for which the static friction response would be reliable. Hence, we will base the final assesment on frictional properties purely on the dynamic friction force.

0.6.4 Out of plane buckling

The thesis builds on the idea that the kirigami configurations will buckle out of plane when stretched. Hence, we should verify this.

Vacuum test at $T = 5$K. We see that the popup and honeycomb pattern buckles considerable out of plane during the stretch while the noncut sheet only experiences minor buckling of ~ 2 Å which is on the same scale as the atomic spacing in the sheet. We also notice that the popup pattern experiences buckles more in consideration to the min and max peaks while the 1%, 99% quartiles is on the same scale as the honeycomb. By looking at the visualization (include this somewhere) we can conclude that this is mainly due to the fringes of the sheet "flapping" around.

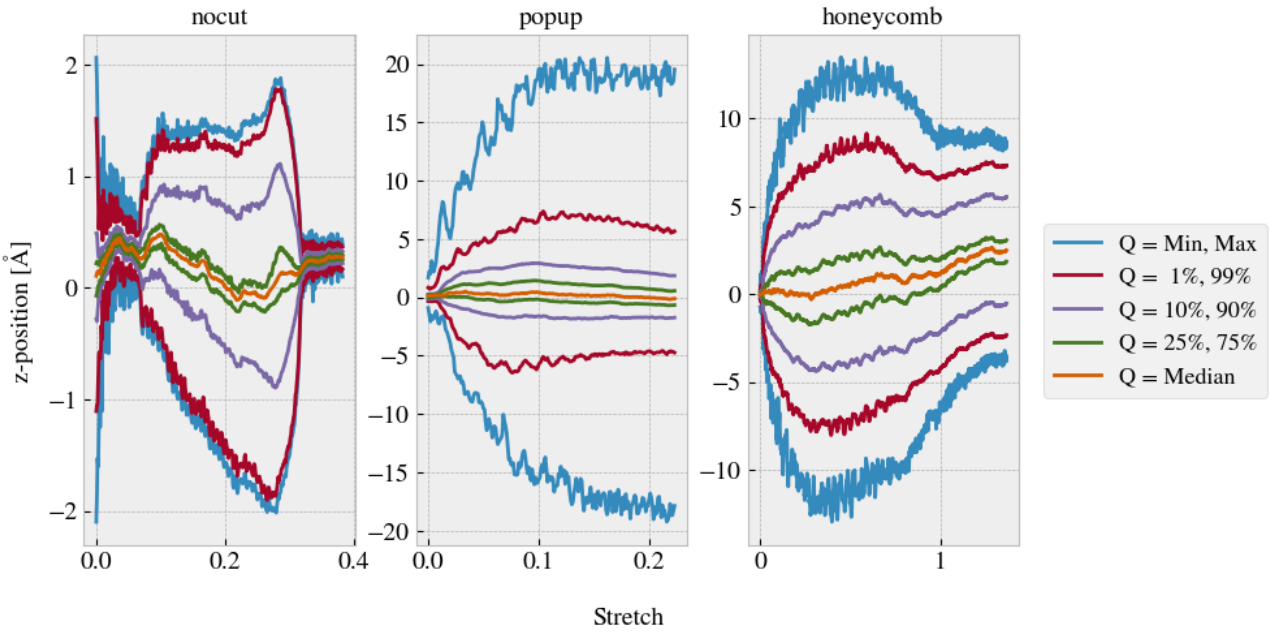

Figure 9: Out of plane buckling during stretch of sheets in vacuum at $T = 5$ K. Reading from left to right the vacuum rupture stretch are 0.38, 0.22 and 1.37.

Similar test is performaned in the presence of the substrate under a higher temperature $T = 300$ K. We assess the contact area by the relative amount of atoms in the sheet within chemical range of the substrate. The cut-off for this interaction is 4 Å corresponding to $\sim 120\%$ the LJ equilibrium distance. Since the contact area is usually calculated as the amout of atoms in contact multiplied with an associated area for each contact this feature is proportional to that.

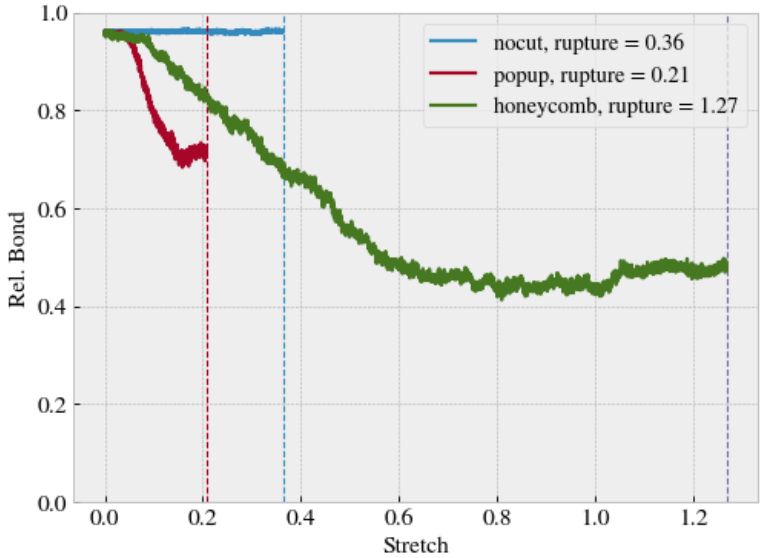

Figure 10: Contact vs. stretching of the sheet, where the contact is measured by the relative amount atoms in the sheet within chemical interaction range to the substrate. The cut-off for this interaction range is 4 Å corresponding to $\sim 120\%$ the LJ equilibrium distance. $T = 300$ K

0.6.5 Investigating selected parmeters

Investigate effects of temperature, drag speed, spring constant and dt.

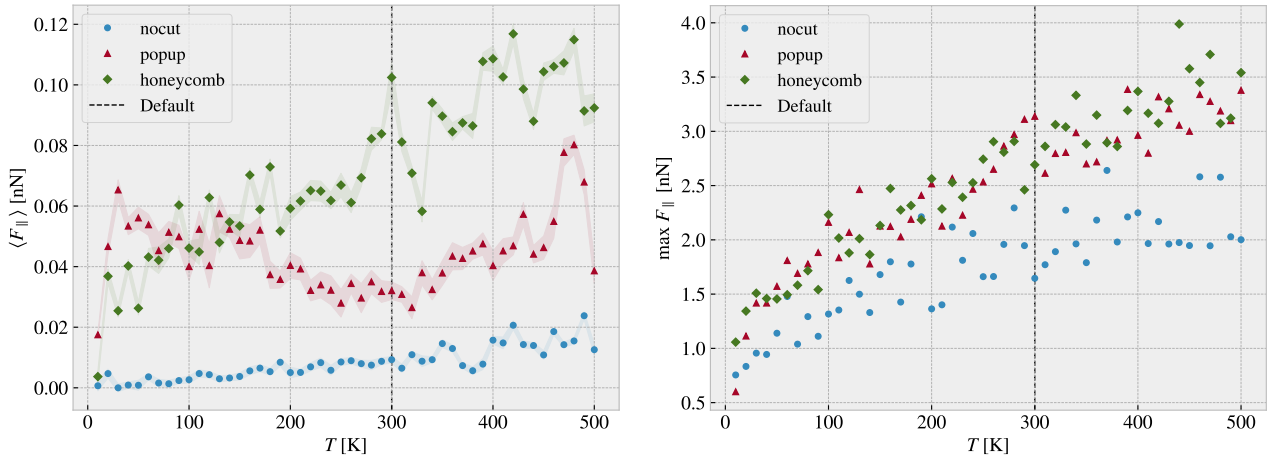

(a) mean friction **(b)** max friction

Figure 11: Temperature. $v = 20$ m/s and fixmove.

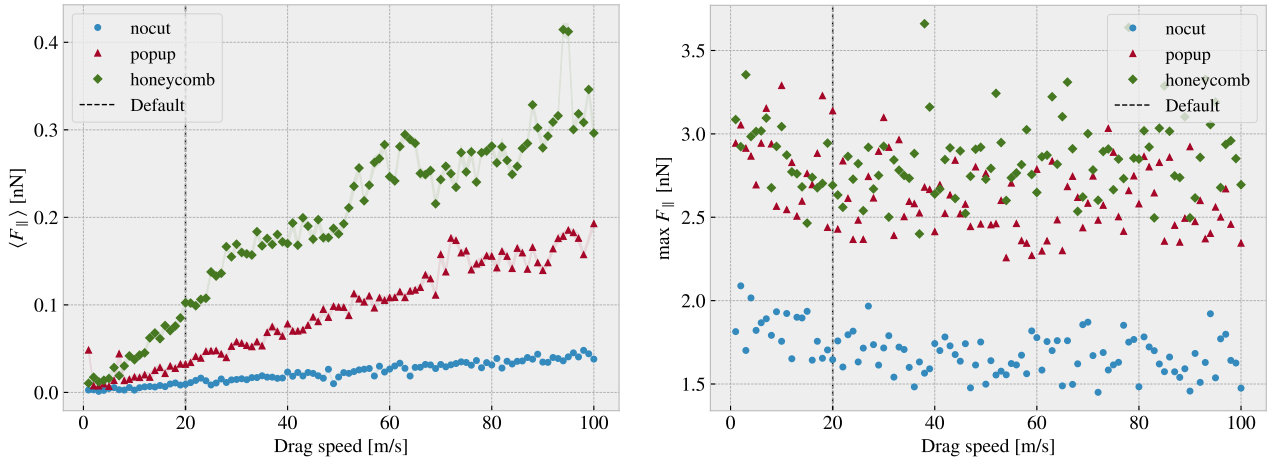

(a) mean friction **(b)** max friction

Figure 12: Drag speed

Simulations of concentric nanotubes in relative motion (telescopic sliding), have revealed the occurrence of well-defined velocities at which friction is enhanced, corresponding to a washboard frequency resonating with longitudinal [172] or circular [173] phonon modes, leading to enhanced energy dissipation. The frictional response becomes highly non-linear while approaching the critical velocity and, contrary to macroscopic systems, washboard resonances can arise at multiple velocities, especially for incommensurate interfaces where more than one length scale may be in common to the contacting surfaces [172] [6].

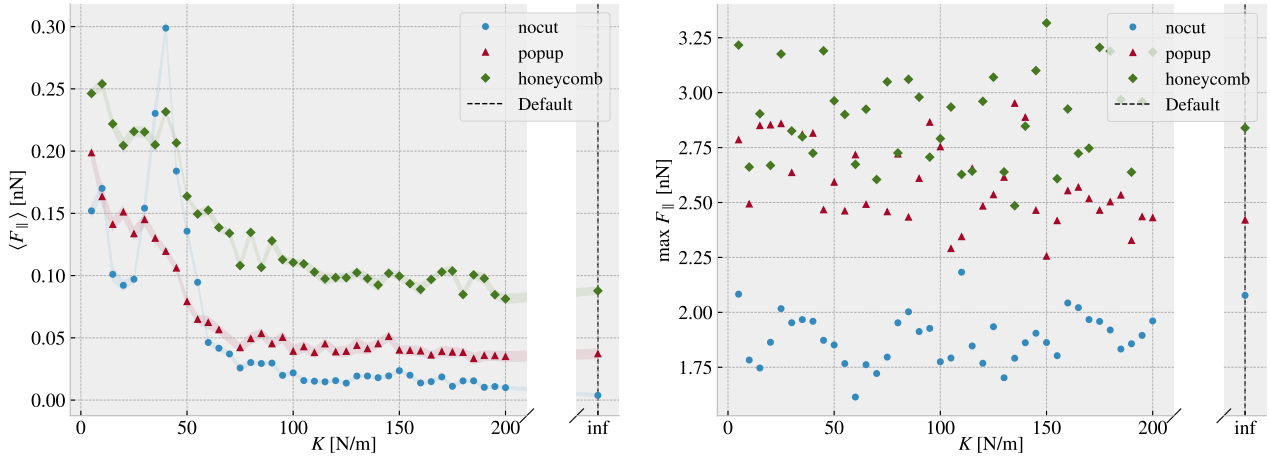

(a) mean friction **(b)** max friction

Figure 13: Spring constant

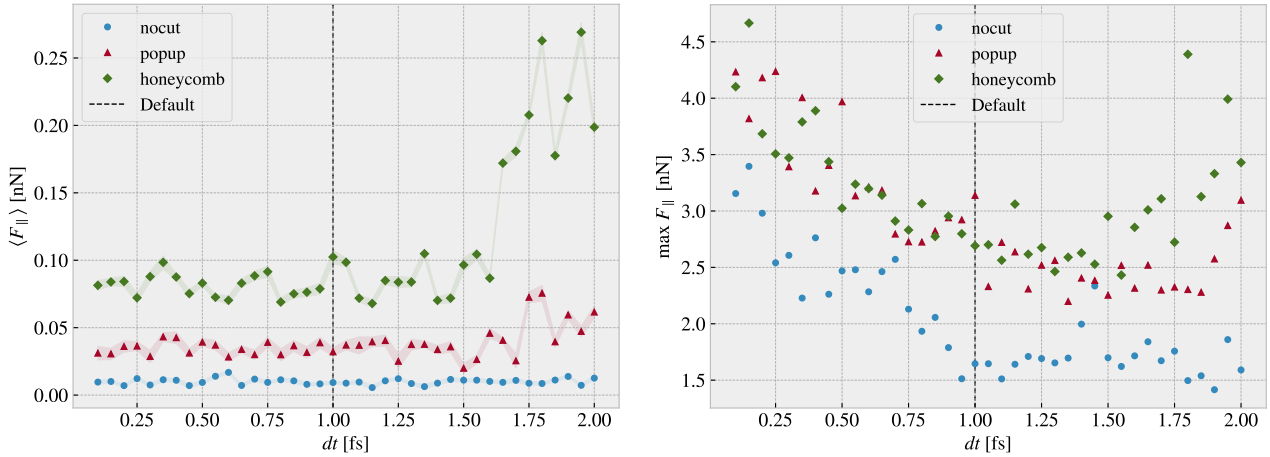

(a) mean friction **(b)** max friction

Figure 14: Timestep

0.6.6 Normal force and stretch dependencies

0.6.6.1 Multi stretch

text

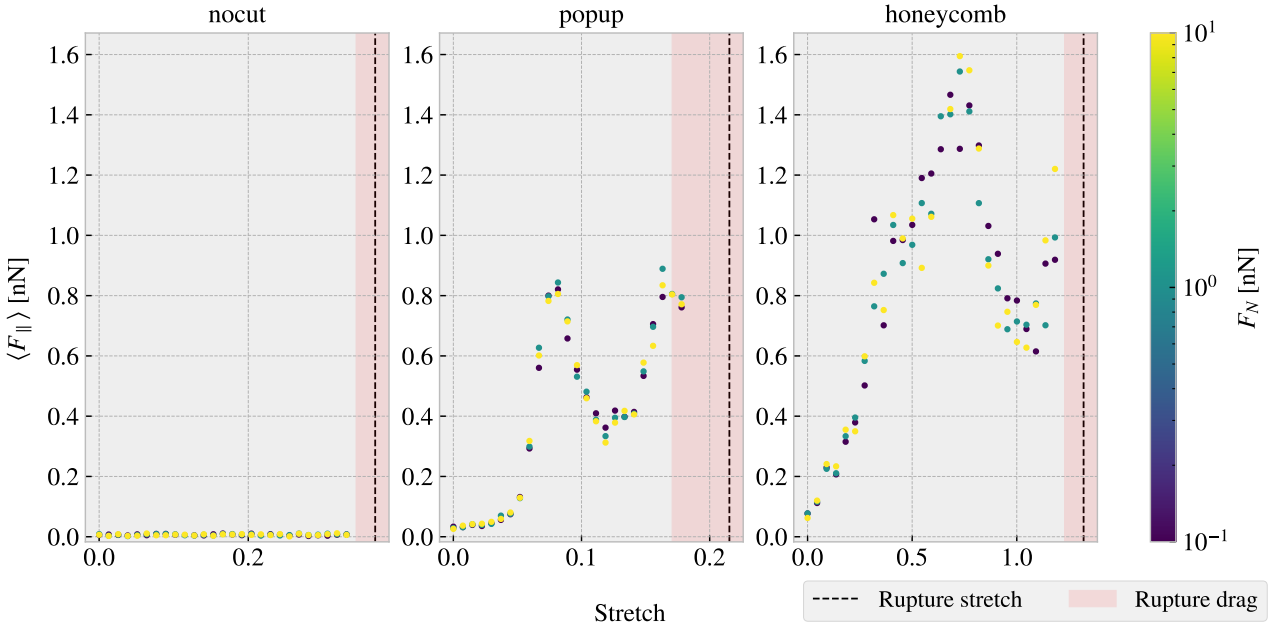

Figure 15: ...

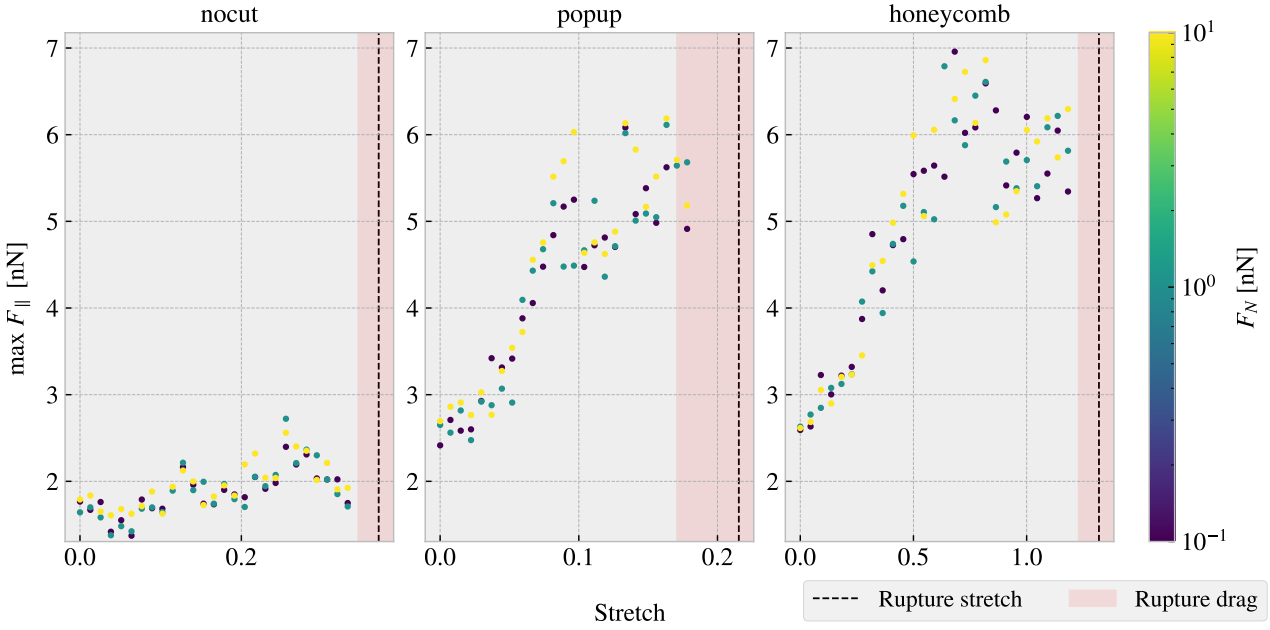

Figure 16: ...

0.6.6.2 Multi normal force

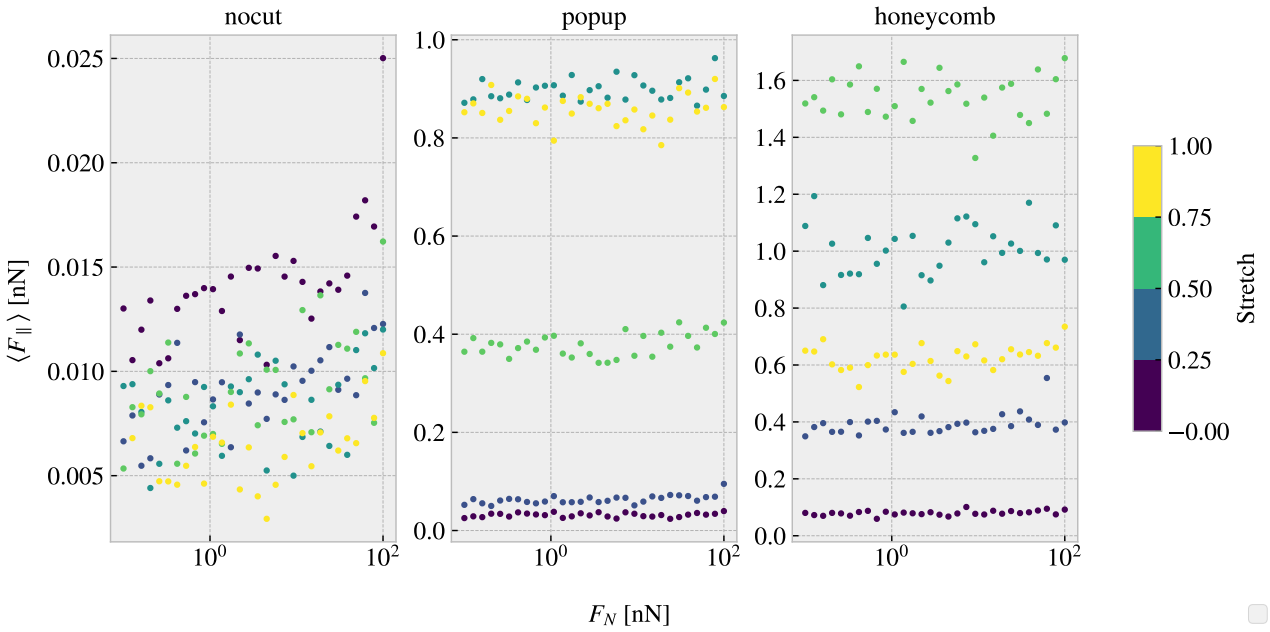

Figure 17: ...

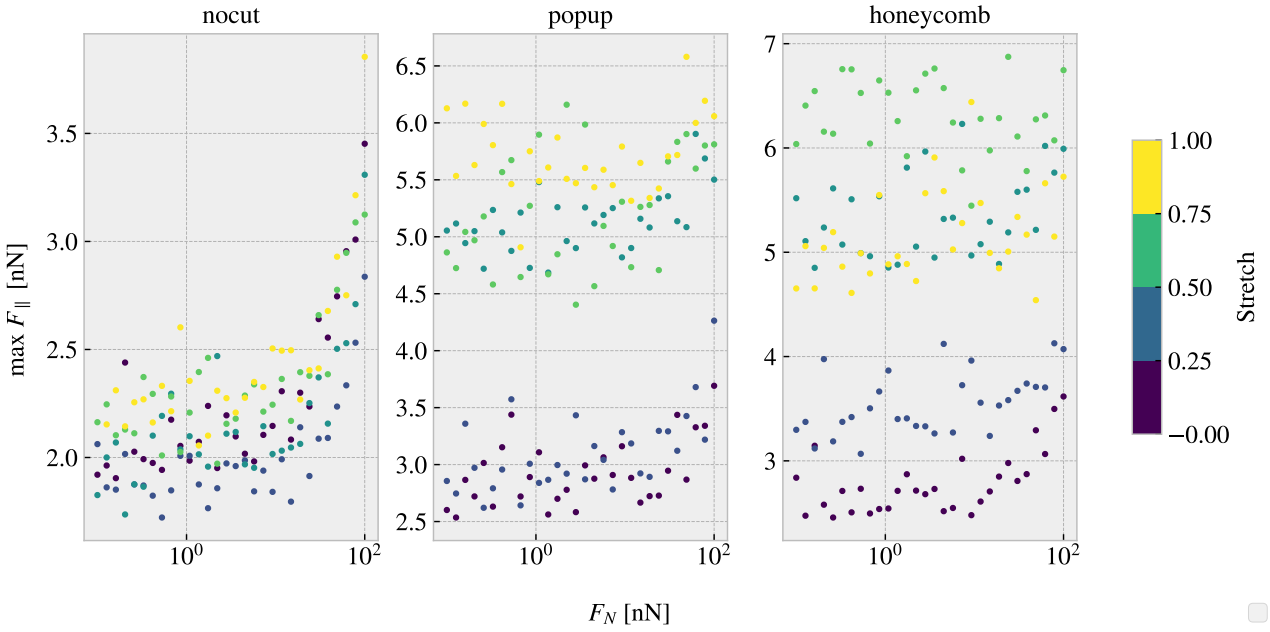

Figure 18: Colorbar is only fitted for the right plot (honeycomb)... this should be fixed. Should I have run a linear distribtion of FN so I could plot it linear here also...?

Table 3: Mean friction coeff

nocut	$0.00009 \pm 1 \times 10^{-5}$	$0.00005 \pm 1 \times 10^{-5}$	$0.00004 \pm 1 \times 10^{-5}$	$0.00005 \pm 2 \times 10^{-5}$	
popup	$0.00005 \pm 3 \times 10^{-5}$	$0.00024 \pm 5 \times 10^{-5}$	$0.0002 \pm 2 \times 10^{-4}$	$0.0005 \pm 1 \times 10^{-4}$	$0.0003 \pm 2 \times 10^{-4}$
honeycomb	$0.00013 \pm 6 \times 10^{-5}$	$0.0006 \pm 3 \times 10^{-4}$	$0.0004 \pm 6 \times 10^{-4}$	$0.0007 \pm 6 \times 10^{-4}$	$0.0009 \pm 3 \times 10^{-4}$

Table 4: Max friciton coeff

nocut	$0.0139 \pm 9 \times 10^{-4}$	$0.0083 \pm 7 \times 10^{-4}$	$0.010 \pm 1 \times 10^{-3}$	$0.0105 \pm 9 \times 10^{-4}$	
popup	$0.007 \pm 2 \times 10^{-3}$	$0.010 \pm 2 \times 10^{-3}$	$0.007 \pm 2 \times 10^{-3}$	$0.009 \pm 3 \times 10^{-3}$	$0.006 \pm 2 \times 10^{-3}$
honeycomb	$0.010 \pm 1 \times 10^{-3}$	$0.007 \pm 2 \times 10^{-3}$	$0.007 \pm 3 \times 10^{-3}$	$0.000 \pm 3 \times 10^{-3}$	$0.004 \pm 3 \times 10^{-3}$

The friction probably does not increase with normal force at an expected rate due to the fact the normal force is only applied on the pull blocks. Especially with the cutted sheet the tension drops such that the effecive normal force on the inner sheet is not changing so much. By this theory the friction force vs. normal force on the pull graph look a bit more like expected.

When looking at the graphs for the PB the max friction is visually textbook linear, while the mean friction is a bit more linear but also with negativ coefficients.

0.6.6.3 Contact area

Show plots of contact area vs stretch and discuss the fact that friction actually increases while contact area drops. Is the conclusion that there might be another more dominant cause of the increasing friction.

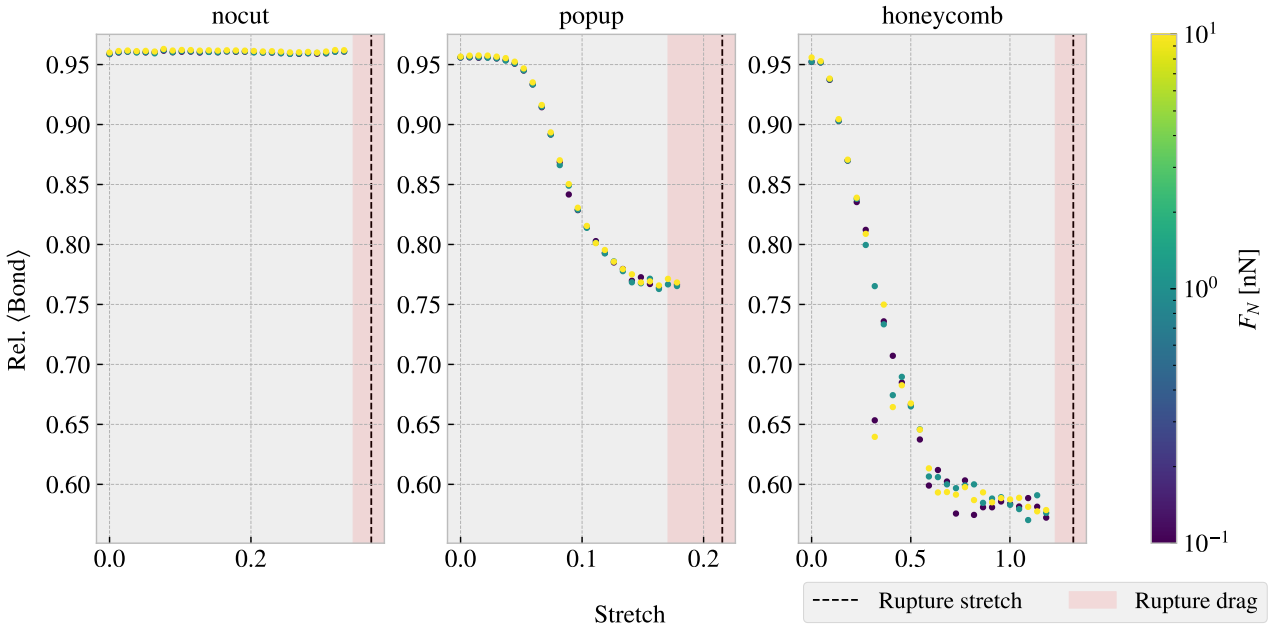

Figure 19

0.6.7 Computational cost

Talk about the computatonal cost of different choices. How does comutation time scale with drag speed, dt and maybe T and K as well. One could also mention scaling with system size.

Show how the number of cores per simulation scale to argue that running on just one core (maybe 4) is smart for the next step of many simulations.

Mention the trouble with GPU to show that this was considered.

0.7 Generating data

Present the configuration and variable choices for the generated dataset. Perhaps include appendix with all the configurations shown in a grid or something similar.

0.8 Training forward network

0.9 Inverse design

0.10 Negative friction coefficient

0.10.1 Simulated coupling of normal force and stretch

0.10.2 Nanomachine coupling

Attempt to couple normal force and stretch by crossed carbon nanotube (CNT) contraption 20.

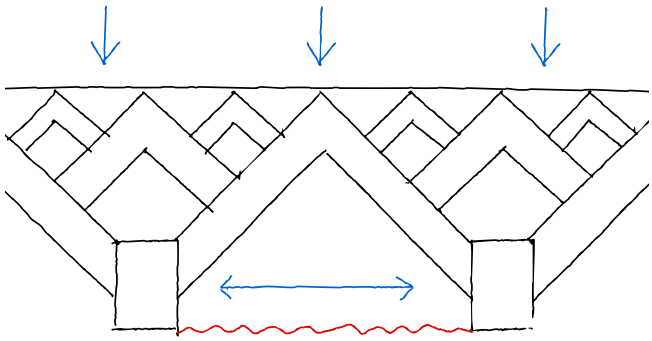

Figure 20: Working sketch for nanomachine

Appendices

Appendix A

Bibliography

[1] E. Gnecco and E. Meyer, *Elements of Friction Theory and Nanotribology*. Cambridge University Press, 2015, 10.1017/CBO9780511795039.

[2] Bhusnan, *Introduction*, ch. 1, pp. 1–? John Wiley & Sons, Ltd, 2013. https://onlinelibrary.wiley.com/doi/pdf/10.1002/9781118403259.ch1. https://doi.org/10.1002/9781118403259.ch1.

[3] H.-J. Kim and D.-E. Kim, *Nano-scale friction: A review*, .

[4] K. Holmberg and A. Erdemir, *Influence of tribology on global energy consumption, costs and emissions*, .

[5] P. Z. Hanakata, E. D. Cubuk, D. K. Campbell and H. S. Park, *Forward and inverse design of kirigami via supervised autoencoder*, *Phys. Rev. Res.* **2** (Oct, 2020) 042006.

[6] N. Manini, O. M. Braun, E. Tosatti, R. Guerra and A. Vanossi, *Friction and nonlinear dynamics*, *Journal of Physics: Condensed Matter* **28** (jun, 2016) 293001.